IEEE Access
Multidisciplinary | Rapid Review | Open Access Journal

Received July 5, 2018, accepted August 13, 2018, date of publication August 16, 2018, date of current version September 7, 2018.

Digital Object Identifier 10.1109/ACCESS.2018.2865799

Feasibility of ALOS2 PALSAR2 Offset-Based Phase Unwrapping of SAR Interferogram in Large and Complex Surface Deformations

WON-KYUNG BAEK, HYUNG-SUP JUNG, (Senior Member, IEEE), AND SUNG-HO CHAE
Department of Geoinformatics, University of Seoul, Seoul 02504, South Korea

Corresponding author: Hyung-Sup Jung (hsjung@uos.ac.kr)

This work was supported by the Korea Meteorological Administration Research and Development Program under Grant KMI2017-9060.

ABSTRACT The interferometric synthetic aperture radar (InSAR) is a well-known tool for mapping ground surface deformations with centimeter precision, and is much better than that used in the offset tracking method. However, the InSAR method has difficulties in precisely measuring large deformation signals because the phase unwrapping can include severe errors in the case of large and complex deformations. To overcome this drawback, an offset-based unwrapping strategy was proposed. However, this strategy has almost never been used for the unwrapping approach because the accuracy of offset measurement is much lower than that of InSAR measurement. As the spatial resolution of the SAR image becomes more precise, the offset measurement accuracy increases. Specifically, the L-band ALOS2 PALSAR2 sensor has much higher offset measurement accuracy due to its higher spatial resolution. In this paper, the feasibility of the unwrapping of a PALSAR-2 interferometric phase with large surface deformation signals, using an offset map, is proved. This validation of offset-based unwrapping was performed using two ALOS2 PALSAR2 co-seismic pairs in the 2016 Kumamoto earthquake where large deformations of more than 200 cm occurred. The offset-based unwrapping was more successful than traditional unwrapping. The root-mean square errors of offset-based unwrapping using GPS *in situ* data were about 1.96 and 1.90 cm in the ascending and descending pairs, respectively. The validation results showed that the ALOS2 PALSAR2 offset-based unwrapping enables us to measure complex and large deformation signals accurately. Precise measurements in high-gradient and high-decorrelated deformation areas would be helpful to better understand geological mechanisms.

INDEX TERMS ALOS2 PALSAR2, synthetic aperture radar, synthetic aperture radar interferometry, offset-based phase unwrapping.

I. INTRODUCTION

Large surface deformations are a global issue and are a frequent occurrence. Earthquakes, such as the 2008 Mw 8.0 Wenchuan earthquake, the 2010 Mw 7.0 Haiti earthquake [1], [2], the 2011 Mw 9.0 Tohoku-Oki earthquake [3], the 2014 Mw 6.0 Napa earthquake [4] and the 2016 Mw 7.0 Kumamoto earthquake [5]–[10], as well as volcanic eruptions, such as the 2005 Sierra Negra volcano eruption [11], Kilauea volcano eruption [12]–[14], and Okmok Volcano eruption [15] affect a significant number of people and can cause extreme damage. These large deformations can reach more than 3 meters and can be spatially distributed up to several hundred kilometers. For example, in the case of the 2010 Haiti earthquake, the surface deformations reached about 2 m, and more than 300,000 persons were confirmed dead or missing and about 250,000 residences and 30,000 commercial buildings were severely broken [16].

Synthetic aperture radar (SAR) interferometry has been widely used to map surface deformations over large areas covering thousands of square kilometers. It is well-known that interferometric SAR (InSAR) is a unique tool capable of measuring surface deformations to an accuracy of several millimeters to centimeters [17], [18] by converting the interferometric phase into surface deformation. However, since the interferometric phase is represented by the wrapped value of ($-\pi$ to π), the InSAR method needs a phase unwrapping procedure. Phase unwrapping is based on the assumption that the phase difference between adjacent pixels has to be within 2π.

Many methods have been developed for phase unwrapping [11], [18]–[21]. Most unwrapping methods have been well applied to normal SAR interferogram cases, but they have difficulties in unwrapping the interferometric phase in extreme cases with complex and steep surface deformations because the phase difference between adjacent pixels can exceed 2π. Even if the phase difference is within 2π, unwrapped values can be mis-estimated if the deformations are very complex and steep. Normally, since surface deformations near fault lines are complex and steep, it is very difficult to measure the deformation magnitude near fault lines [19].

The offset-tracking method is a well-known tool used to measure surface deformations, which is usually done by using the intensity cross-correlation approach. The method does not require the unwrapping process, but has an accuracy at least several times lower than the InSAR method because the offset accuracy is a function of the spatial resolution (∼meters), while the InSAR accuracy largely depends on the radar's wavelength (∼centimeters). Despite this, the offset method has been successfully applied to the observation of fast moving glaciers or large earthquake [22]–[25]. As recent satellite radar sensors, such as the X-band TerraSAR-X and the L-band Advanced Land Observing Satellite 2 (ALOS2) PALSAR2, have higher spatial resolutions, the measurement performance of the offset method is remarkably improved using recent satellite images [25], [26]. Nevertheless, it is obvious that the offset method still has inferior accuracy compared to the InSAR method.

In summary, in complex and large deformation areas, (i) the InSAR method is not applicable to large deformations due to the phase unwrapping errors, and (ii) the offset-tracking method works well, although it has a much lower accuracy. Using the trade-off between InSAR and offset measurements, an offset-based phase unwrapping method was proposed. However, it has almost never been used for the unwrapping approach because offset accuracy is much lower than the InSAR accuracy.

In this study, we tested the feasibility of the offset-based phase unwrapping by successfully applying it to ALOS2 PALSAR2 interferograms which exhibit large and complex surface deformation signals. For the feasibility test, two ALOS2 PALSAR2 co-seismic pairs in the 2016 Kumamoto earthquake were used, where significant deformation of more than 200 cm occurred.

For optimal offset-based unwrapping, the non-local (NL) means filter and multi-kernel offset-tracking methods were applied to the estimated offset map. The feasibility validation of the offset-based unwrapping was performed by using GPS in-situ measurements. The offset-based unwrapping results were compared with minimum cost flow (MCF) unwrapping. Moreover, the unwrapping performance in steep deformation slope areas was described in detail. It was proved that the proposed offset-based phase unwrapping approach enables the accurate observation of large and complex surface deformations.

II. METHODOLOGY

The InSAR phase includes the deformation signal and topography-related signal, as well as the error components, such as thermal noise, temporal and geometrical decorrelations, etc. [27]. These error components degrade the accuracy of the surface deformation measurement and produce unwrapping errors, because phase jumps between adjacent pixels normally occur in noisy SAR images [19], [28]. To suppress the noise components, Goldstein's adaptive filter can be applied to the noisy SAR image [29], [30], and hence, valid deformation signals may be estimated by unwrapping the noise-reduced image [29], [31], [32].

Nevertheless, it is almost impossible to unwrap a complex and steep surface deformation phase because the phase difference between adjacent pixels can exceed 2π. Even if the phase difference is within 2π, unwrapped values can be mis-estimated. Many researchers have made efforts to overcome the problem [11], [20], [33]. One well-known solutions is to unwrap the residual phase after a complex and large deformation phase is subtracted from a low-frequency and low-accuracy measurement, such as the offset-tracking measurement. It is almost impossible to apply this to SAR interferometric data because the offset-tracking measurement has much lower precision with respect to the radar wavelength, which corresponds to a phase difference of 4π.

Recently, the L-band ALOS2 PALSAR2 data has achieved higher spatial resolution (less than 4 m); moreover, the multi-kernel offset-tracking method has an improved accuracy (about 5.4 cm) [25]. These improvements may enable the application of the offset-based unwrapping concept to PALSAR2 data, because the accuracy is two times smaller than half of the L-band radar wavelength (about 11.9 cm). In this study, the feasibility of the offset-based unwrapping was tested to determine whether it is applicable to PALSAR2 InSAR pairs. Fig. 1 shows the workflow for the offset-based phase unwrapping approach used in this study. The processing steps are as follows:

1. Generation of the wrapped differential interferogram;
2. Generation and filtering of the range offset map;
3. Generation of the unwrapped residual interferogram; and
4. Creation of the unwrapped differential interferogram.

The wrapped differential interferogram can be generated by the traditional InSAR processing method, which is composed of three main steps: 1) generation of the master and slave SLC images through azimuth common band filtering, 2) co-registration between the master and slave SLC images at a sub-pixel level, and 3) generation of the differential InSAR interferogram via the flat-Earth and topographic phase correction using the Shuttle Radar Topography Mission (SRTM) DEM. More details of the InSAR processing can be found in [18], [26], and [34]. For the PALSAR2 data, it should be noted that the co-registration is carefully processed because it is the most important processing step. Especially for high mountain areas, the interferometric coherence can be degraded if the co-registration is not processed precisely.

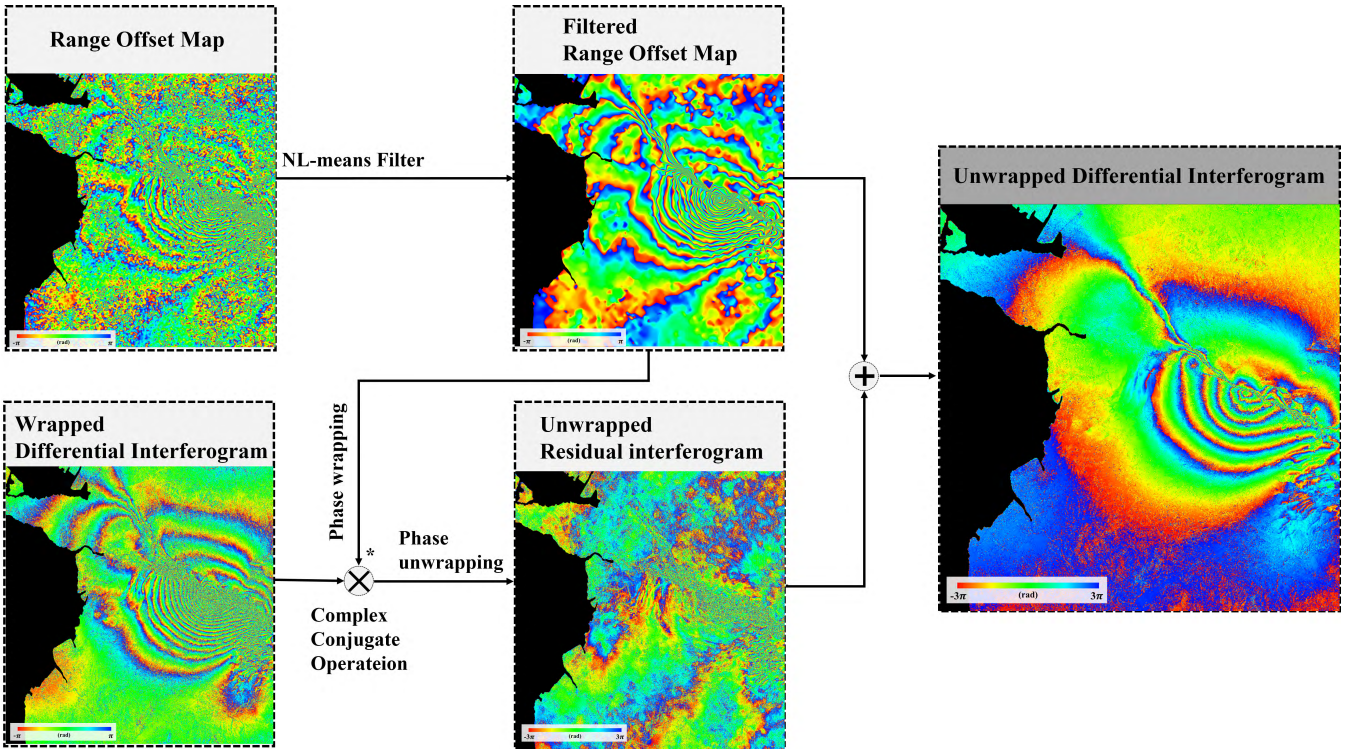

FIGURE 1. Detailed workflow for the proposed offset-based phase unwrapping approach.

The range offset map can be generated by the multi-kernel offset-tracking method [25]. The method estimates multiple offset values from the cross-correlation operation using the multi-window kernel, which is composed of small to large window kernels. It then measures a final offset value by averaging the estimated multiple offsets after outliers are removed by using a set confidence level [25]. The method exploits the fact that the small kernels provide more accurate measurements for large and complex deformation signals, while the larger kernels are better for smooth deformation signals. Although the method has better accuracy than more traditional methods, there is some difficulty in applying the range offset map to generate the residual interferogram because the noise level of the range offset map is high. The NL-means filter was used for noise suppression in the range offset map. The NL-means filter has the advantage of the filter reducing the noise components and preserving the edge information [35], [36]. In addition, the range offset map can require a topographic correction. Topographic offset distortion is caused by significant topographic height variations. It is linearly proportional to the perpendicular baseline, as well as the topographic height. Thus, if the perpendicular baseline is large, and the topographic height is high, the topographic distortion is severe and hence requires removal from the range offset map. Moreover, the NL-means filtered offset map requires conversion from pixels to radians.

The residual interferogram is generated by the following two steps: i) the filtered offset map is wrapped by 2π and ii) the wrapped differential interferogram is multiplied by the complex conjugate of the wrapped filtered offset map. Since the residual interferogram must be very smooth, the residual interferogram can be easily unwrapped by a traditional algorithm such as MCF [31]. After the residual interferogram has been unwrapped, the unwrapped differential interferogram can be obtained by adding the unwrapped residual interferogram to the filtered range offset map.

As mentioned previously, the feasibility of the offset-based unwrapping approach largely depends on the precision of the filtered range offset map. If the precision is poor due to a high perpendicular baseline or/and temporal decorrelations, the approach is not applicable. Moreover, the required precision should be smaller than half the radar wavelength (2π). The shorter the sensor wavelength is, the higher the required precision is. This means that X-band interferometry requires a better precision than L-band interferometry. Since a phase of 2π in the L-band PALSAR2 data corresponds to about 11.9 cm, the minimum required precision of the offset map for offset-based unwrapping should be smaller than 11.9 cm. Normally, the minimum requirements of X- and C-band radar interferometry are approximately 1.5 cm and 2.5 cm, respectively, and hence, it is difficult to apply the offset-based unwrapping approach to X- and C-band radar interferometric pairs. Therefore, the offset-based method is more appropriate to L-band PALSAR2 interferometry.

III. DATASET USED

Two ALOS2 PALSAR2 interferometric pairs were used to test the feasibility of the offset-based unwrapping

approach. The ALOS2 satellite was launched in May 2014 and mounted with an L-band radar sensor, PALSAR2. The PALSAR2 was significantly upgraded from PALSAR, and hence, has a higher spatial resolution. The PALSAR2 has three modes: stripmap, scanSAR and spotlight. In this study, we used the PALSAR2 images obtained through the stripmap mode. Table 1 summarizes the system parameters of the PALSAR2 stripmap images used for this test. The PALSAR2 has a large chirp bandwidth of 84.0 MHz, which indicates that the range spatial resolution was remarkably improved to about 2.4 m, compared to PALSAR. The improvement enables the application of the offset-based method to the PALSAR2 data. The PALSAR2 test data were obtained from the 2016 Mw 6.5 and Mw 7.3 Kumamoto earthquakes. Since a lot of large and complex deformation areas existed in the test data, the data was ideal to validate the performance of the offset-based unwrapping approach.

TABLE 1. System parameters of ALOS 2 PALSAR 2 stripmap data used for this study.

Parameters	PALSAR 2
Effective azimuth antenna dimension (m)	9.9
Effective Doppler Bandwidth (Hz)	1515
Pulse repetition frequency (Hz)	2000
Chirp bandwidth (MHz)	84.0
Carrier frequency (GHz)	1.258
Azimuth resolution (m)	3.8
Ground range resolution (m)	2.4

The PALSAR2 interferometric pairs are listed in Table 2. The test data was selected by considering the perpendicular and temporal baselines. Two interferometric pairs with short baselines were selected, as listed in Table 2. The two interferometric pairs were 20160211_20160602 in the ascending orbit and 20160307_20160418 in the descending orbit. The perpendicular baselines were about −74 and −122 m in the ascending and descending orbits, respectively. The temporal baselines were 112 and 42 days in the ascending and descending acquisitions, respectively. The differential interferograms generated from the pairs had higher coherences due to the short perpendicular and temporal baselines.

TABLE 2. Interferometric parameters of PALSAR2 pairs used for this test.

Pairs	Track No.	Acquisition Date	Perpendicular baseline (m)	Temporal baseline (days)
Ascending	130	11/02/2016 02/06/2016	-74	112
Descending	23	07/03/2016 18/04/2016	-122	42

IV. RESULTS

The offset-based unwrapping strategy was applied to the 2016 Mw 6.5 and Mw 7.0 Kumamoto earthquakes to validate the performance of the method. A moderate earthquake of Mw 6.5 occurred on April 14, 2016. The depth of the epicenter was shallow (about 11 km). A larger earthquake of Mw 7.3 occurred on April 16, 2016 [6]–[10]. It is known that the earthquakes were generated on a right-lateral strike-slip fault; subsidence of about 2.1 m and horizontal displacement of about 2.0 m were observed [7]–[10].

Two co-seismic interferometric pairs were obtained from the event (Table 2). The wrapped differential interferogram was generated by the following procedure: i) common band filtering was applied to the PALSAR2 SLC images in the azimuth direction to reduce the decorrelation factor due to different Doppler centroids [16], [25], ii) the offset parameters of the master and slave SLC images at a sub-pixel level were calculated, iii) the slave SLC image was resampled into the coordinates of the master SLC image using the offset parameters, iv) an interferogram was generated by the complex conjugate operation of the master and resampled slave SLC images with range common band filtering, v) a synthetic interferogram was simulated from the SRTM DEM to correct the flat-Earth and topographic phases, vi) a wrapped differential interferogram was created by subtracting the synthetic interferogram from the interferogram and multilooked by 12 × 15 looks (about 30 × 30 m) in the range and azimuth directions to reduce the phase noise [30], vii) the wrapped differential interferogram was filtered by Goldstein's adaptive filter with a window size of 32 and the smoothing parameter of 0.5 [30].

Fig. 2 shows the wrapped differential interferograms acquired from the ascending pair of 20160211 and 20160602, and the descending pair of 20160307 and 20160418, respectively. The gradient of the fringe was very steep due to the large co-seismic deformation (Fig. 2). The area of steepest surface deformation were found near the fault lines (Figs. 2(a) and 2(b)). Phase changes of about 88.0 rad. (28 π) and 37.7 rad. (12 π) were estimated from the ascending and descending differential interferograms, respectively. However, the phase could not be properly measured because it was not possible to unwrap the extremely steep and complex deformation area. Moreover, deformation patterns in the

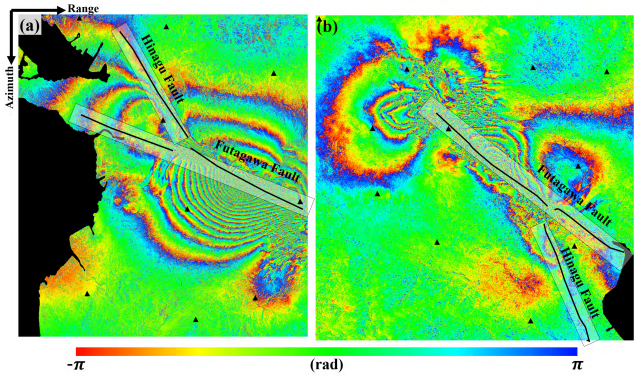

FIGURE 2. Wrapped differential interferograms: (a) the ascending pair of 20160211 and 20160602 and (b) the descending pair of 20160307 and 20160418; the black triangles are the locations of GPS stations and the solid line indicates the Hinagu and Futagawa fault lines.

decorrelated areas close to the fault lines could not be recognized due to high-gradient deformation patterns. Although maximum deformations of about 2 m were observed in both the horizontal and vertical directions [5], [8], [9], valid deformations could not be measured from the differential interferograms.

To overcome these problems, the multi-kernel offset tracking method was applied to the ascending and descending interferometric pairs [25]. A total of sixteen multi-kernels, from 32×32 to 256×256, were used for offset tracking. The kernel sizes used were 32, 64, 128 and 256 in both the range and azimuth directions. After outliers were removed from the 16 offset measurements by using the 95% confidence level, the final offset measurement was estimated by averaging the remaining offsets. More details can be found in [25].

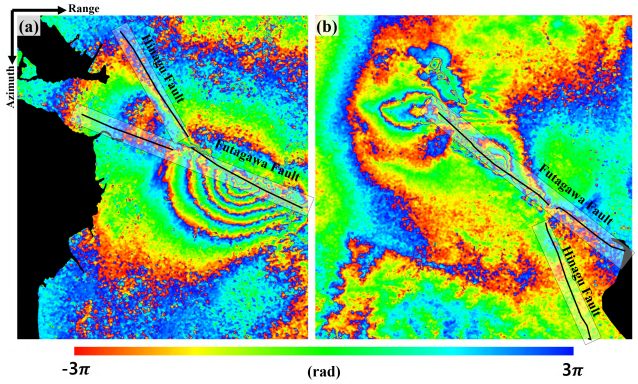

FIGURE 3. Range offset maps estimated by the multi-kernel based offset tracking method: (a) ascending pair of 20160211 and 20160602 and (b) descending pair of 20160307 and 20160418.

Fig. 3 shows the range offset map estimated by the multi-kernel offset tracking method, after conversion from pixels to radians. As shown in Fig. 3, topography-related offset components could be found from the offset maps. The descending offset map (Fig. 3b) is more severely affected by topography than the ascending offset map (Fig. 3a), because the perpendicular baseline of the descending pair is approximately two times larger than that of the ascending pair. Since the topographic effect is linearly proportional to the topographic height, the effect of topography can be removed using a linear regression method.

Fig. 4 shows the topography-corrected range offset maps acquired from the ascending and descending orbits. Valid deformation signals were measured from the offset maps, even in the decorrelated areas close to the fault lines. It is well known that the InSAR method cannot measure high-gradient deformation signals, while the offset tracking method can. Maximum phase changes of about 145.5 rad and 133.9 rad. were observed from the ascending and descending offset maps, respectively. The maximum phase value differences between the offset maps and differential interferograms were as much as 57.5 rad. and 96.2 rad from the ascending and descending offset maps, respectively. These differences were due to the inability to measure the deformation phase from

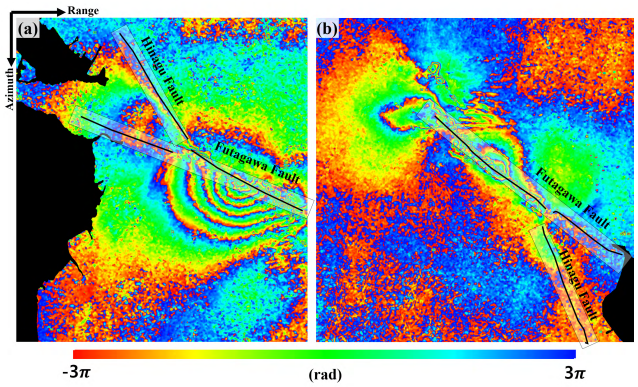

FIGURE 4. Topography-corrected range offset maps: (a) ascending pair of 20160211 and 20160602 and (b) descending pair of 20160307 and 20160418.

the differential interferograms in the decorrelated areas. The offset maps were found to have higher noise components than the differential interferograms when Figs. 2a and 2b were compared with Figs. 4a and 4b.

As the offset maps had high noise components, the maps could not be used for residual phase calculation without being filtered, because the noise components can interrupt the unwrapping of the residual phase. To confirm the problem, the residual interferograms were 1) calculated by the phase difference between the differential interferograms and the range offset maps, and 2) unwrapped by the MCF algorithm. However, numerous unwrapping errors occurred in the residual interferograms. The hard-weighting Gaussian filter used by [11] caused unwrapping errors in high-gradient deformation edges, local deformation areas, etc. To minimize the drawbacks, the NL-means filter was applied to the range offset maps. Consequently, residual interferograms were generated from the topography-corrected and NL-means filtered range offset maps.

Figs. 5a and 5b represent the NL-means filtered range offset map and unwrapped residual interferogram in the ascending interferometric pair, respectively; Figs. 5c and 5d compare the unwrapped interferograms generated by the offset-based unwrapping strategy and the traditional MCF algorithm. The noise effect of the offset map was significantly reduced Fig. 5a, and the residual interferogram in Fig. 5b was unwrapped with very few unwrapping errors. Since there was a phase difference in the residual interferogram between the differential interferogram and the range offset map, the phase values in the residual interferogram of Fig. 5b must be close to zero. However, the residual interferogram had a long-wavelength pattern, as seen in Fig. 5b, due to ionospheric effects. The deformation signal is not related to the long-wavelength pattern in the residual interferograms while the ionospheric signal remains because the sign of the ionospheric contribution in the range offset map and differential interferogram is different [37]–[39].

The standard deviation of the residual interferogram was about 4.9 rad. As the ionospheric effect is very long-wave,

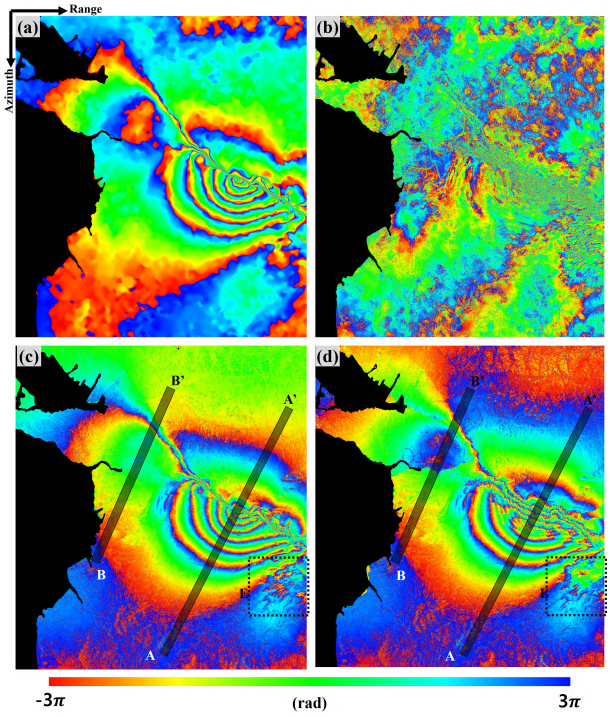

FIGURE 5. Results from the ascending pair, processed by the offset-based unwrapping approach: (a) NL-means filtered range offset map, (b) unwrapped residual interferogram, (c) unwrapped interferogram by the offset-based method and (d) unwrapped interferogram by the traditional MCF algorithm. Profiles AA′ and BB′ are presented in (c) and (d).

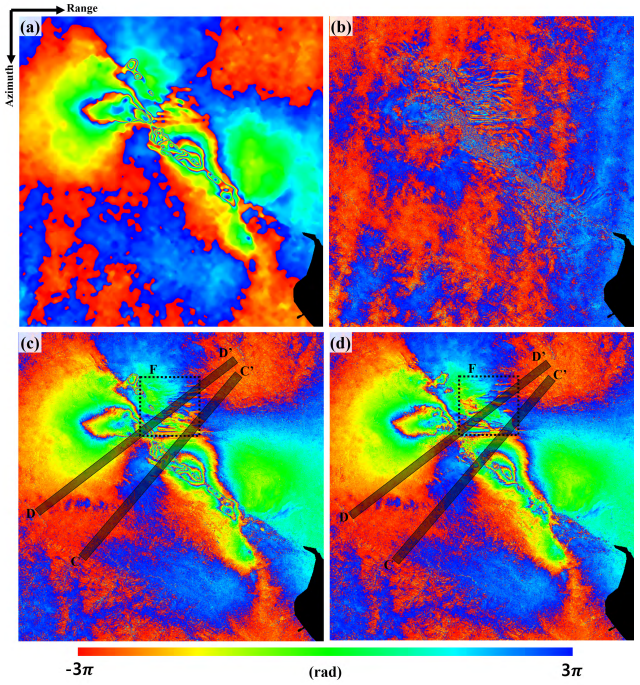

FIGURE 6. Results from the descending pair, processed by the offset-based unwrapping approach: (a) NL-means filtered range offset map, (b) unwrapped residual interferogram, (c) unwrapped interferogram by the offset-based method and (d) unwrapped interferogram by the traditional MCF algorithm. Profiles CC′ and DD′ are presented in (c) and (d).

unwrapping the residual interferograms with ionospheric contributions was facile. However, if the ionospheric turbulence is very severe, the unwrapping may present a challenge. Figs. 5c and 5d represent the differential interferograms which have been unwrapped by the offset-based unwrapping and traditional MCF methods, respectively. The observed maximum deformation signals in the two unwrapped interferograms were about 145.6 rad. and 13.6 rad. in the offset-based unwrapping and traditional MCF methods, respectively. The large discrepancy is because the traditional method could not properly unwrap the high-gradient deformation phase near the fault lines.

Figs. 6a and 6b display the NL-means filtered range offset map and unwrapped residual interferogram from the descending interferometric pair, respectively, and Figs. 6c and 6d compares the unwrapped interferograms generated by the offset-based unwrapping and traditional MCF methods. The noise component was efficiently removed from the range offset map (Fig. 6a). The residual interferogram had a long-wave pattern, but the magnitude of the pattern had a lower phase value, as seen in Fig. 6b. The standard deviation of the residual interferogram was about 1.3 rad, and was approximately 4 times lower than the ascending residual interferogram. This is due to low ionospheric distortion.

The maximum deformations were about 103.0 rad. and 105.5 rad in the filtered range offset map and the offset-based unwrapped differential interferogram, respectively. This indicates that the offset-based method enabled the unwrapping of the interferogram without unwrapping any errors. The maximum deformation from the traditional unwrapped interferogram was approximately 17.6 rad. because the high-gradient deformation phase near the fault lines could not be properly unwrapped, as previously mentioned in the ascending case.

Fig. 7 shows the difference between the two unwrapped interferograms produced by the offset-based and traditional

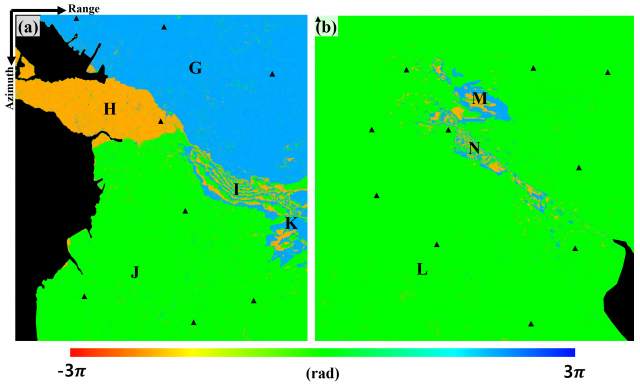

FIGURE 7. Difference maps between the unwrapped interferograms by the offset-based and traditional methods in the (a) ascending and (b) descending acquisitions.

methods. The differences were zero in most areas, as seen in Figs. 7a and 7b. Especially in Fig. 7b, the differences in most areas were almost zero, except for in the areas near the fault line. Nevertheless, the maximum difference was as large as 100.5 rad. at the fault line. The difference corresponds to deformation of about 188.8 cm in the line-of-sight (LOS) direction. This is because high-gradient surface deformations occurred along the fault line and the deformation phase could not be unwrapped correctly. In Fig. 7a, phase jumps were found due to the miscalculation of phase ambiguity numbers in zones H and G (Fig. 7a). The miscalculated phase ambiguity numbers were -2π and -4π in zones H and G, respectively. This is caused by the fault line that crosses the whole interferogram, which is a well-known phenomenon [28]. The maximum difference, observed in the zone I, was about 138.6 rad. which corresponds to LOS deformation of about 260.4 cm.

Fig. 8 compares the difference between the LOS deformations measured from the unwrapped interferograms by the offset-based and traditional methods in the profiles of (a) A-A′, (b) B-B′, (c) C-C′ and (d) D-D′, shown in Figs. 5 and 6.

Fig. 8a shows that the offset-based method was applicable to measure deformation, even in the decorrelated areas. This is because the valid deformation was measured by the offset tracking method, even though the differential interferogram was decorrelated. In profile A-A′, the maximum LOS deformation (∼270.2 cm) was observed by the offset-based method, while the traditional method measured just 131.6 cm; the traditional method could not calculate valid LOS deformation. Profile B-B′ shows the miscalculation of the phase ambiguity numbers in zones H and G of Fig. 7 (Fig. 8b). As previously mentioned, the error is caused by the fault line crossing the whole interferogram. Profile C-C′ confirms that the offset-based method enables the measurement of valid LOS deformation (Fig. 8c).

In this profile (C-C′), the maximum deformation of about 198.2 cm was observed by the offset-based method, while that of about 47.2 cm was measured by the traditional method. It should be noted that the deformation area was only 85 pixels in the range direction, meaning that the deformation gradient was very high in the area. Thus, this further confirms that high-gradient deformation cannot be estimated by the InSAR method, but can be measured by the offset-tracking method. Profile D-D′ (Fig. 8d) includes the 'linear surface rupture' area reported by [6]. The phase discontinuity and high decorrelation due to the steep and complex deformation occurred in the 'linear surface rupture' area, and hence the traditional method did not work correctly. On the other hand, the offset-based method correctly measured the phase discontinuity as well as estimating the LOS deformation in the highly decorrelated area (Fig. 8d).

Fig. 9 enlarges the linear surface rupture areas of boxes E and F, which are shown in Figs. 5 and 6. Some deformation in the areas occurred due to small linear ruptures, and hence, the phase discontinuity and high decorrelation were caused by the deformations, as previously mentioned. Consequently, unwrapping the deformations by

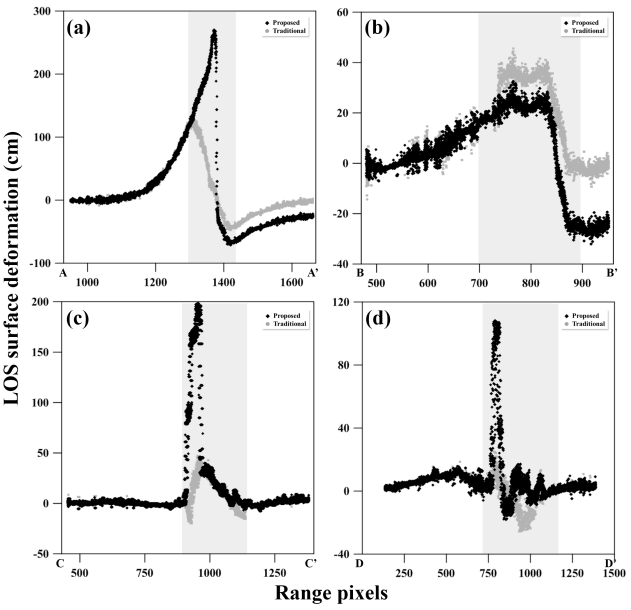

FIGURE 8. Comparison between the LOS deformations measured from the unwrapped interferograms by the offset-based and traditional methods in the profiles of (a) A-A′, (b) B-B′, (c) C-C′ and (d) D-D′. These profiles are shown in Figs. 5 and 6. The black and gray solid circles denote the LOS deformations measured from the offset-based and traditional methods, respectively. The gray zones in Fig. 8 denote areas where large unwrapping errors occurred.

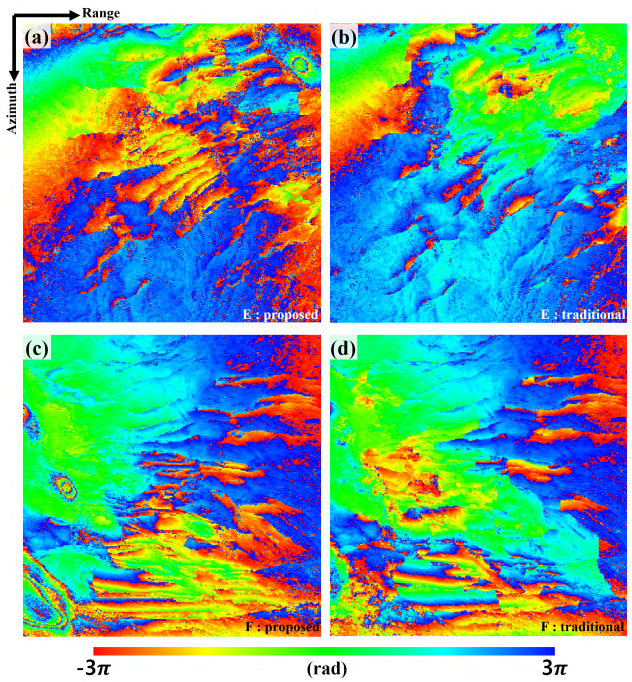

FIGURE 9. Comparison between the phases unwrapped by the offset-based and traditional methods in the areas affected by linear surface ruptures (boxes E and F (Figs. 5 and 6)).

the traditional MCF method caused errors, and the unwrapping errors affected the deformation patterns, as shown in Figs. 9b and 9d. In the interferogram which was unwrapped by the offset-based method, unwrapping errors were found in some areas, but these errors were much reduced compared to the traditional method (Figs. 9a and 9c). While it is well-known that unwrapping complex deformations is not easy [1], [2], [19], the results show that the offset-based method can accurately unwrap the interferometric phase even in complex and steep deformation areas.

Fig. 10 compares the InSAR LOS deformations with GPS-derived LOS deformations for the ascending and descending pairs. The GPS data was provided by the GNSS Earth Observation Network System (GEONET). In the descending pair, the achieved measurement accuracy was about 1.90 cm for the offset-based and traditional methods, as seen in Fig. 10b. This is because in-situ GPS stations do not exist in the high-gradient deformation areas. The measurement accuracies of the ascending pair were about 1.96 cm and 16.84 cm in the offset-based and traditional measurements, respectively (Fig. 10a). The large discrepancy was caused by the phase jumps near the fault lines. Since in-situ GPS measurements did not exist in the high-gradient and highly decorrelated deformation areas, the measurement accuracy in these areas could not be estimated. The measurement accuracies of filtered offset maps were 3.13 and 2.63 cm for ascending and descending pairs. The accuracies were 160 and 138% larger compared to the proposed strategy for ascending and descending pairs respectively. These results show the proposed strategy could accurately reconstruct surface deformation and enhance the measurement accuracy compared to multi-kernel offset-tracking method [11], [25]. In the highly decorrelated areas, close to the fault lines, the accuracy largely depends on the accuracy of the range offset maps. In the high-gradient deformation areas, the accuracy is dependent on the measurement accuracy of the interferograms, but only if the unwrapping processing is adequately completed.

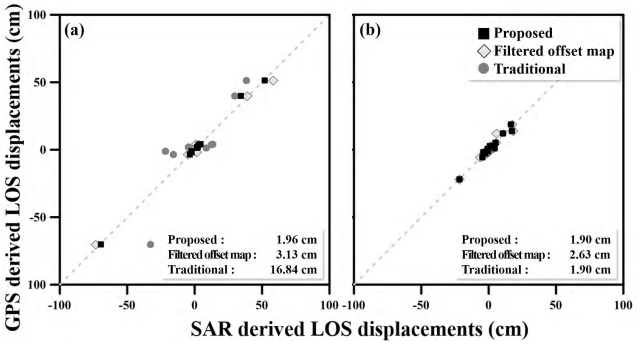

FIGURE 10. Comparison of the InSAR and GPS-derived LOS displacements in the (a) ascending and (b) descending interferometric pairs. The black squares denote the LOS deformations measured by the offset-based strategy. The light grey diamonds show the LOS deformations of the filtered range offset maps. And the dark grey circles show the LOS deformation measured by traditional methods.

The precise measurements in the high-gradient and highly decorrelated deformation areas would be helpful for a better understanding of geological mechanisms. The results showed that the ALOS2 PALSAR2 offset-based unwrapping enabled the measurement of valid deformations even in high-gradient and highly decorrelated deformation areas.

V. CONCLUSIONS

Recently, both satellite radar sensors and interferometric and offset-tracking methods have been modified and improved. In this study, the feasibility of the offset-based unwrapping approach in terms of its effectiveness in unwrapping the interferometric phase of high-gradient surface deformations was tested. The offset-based unwrapping strategy exploits the high spatial resolution of the ALOS2 PALSAR2 SAR imagery and the improved accuracy of the multi-kernel offset-tracking method. The offset-based method was applied to the ascending and descending ALOS PALSAR-2 co-seismic pairs obtained from the 2016 Kumamoto earthquake, to compare the offset-based and traditional unwrapping methods.

To test this methodology, wrapped differential interferograms were generated by a well-known InSAR processor, including azimuth common band filtering, co-registration, interferogram generation, topographic and flat-Earth corrections, multi-looking and filtering. The range offset maps were created by the multi-kernel based offset tracking method. The differential interferograms and range offset maps showed the steep surface deformation near the fault lines. In addition, a topography-related offset component was found in the range offset maps, and hence the topographic effect was corrected from these maps. The noise component was reduced by the NL-means filter. Residual interferograms were generated by subtracting the range offset-derived phase from the differential interferometric phase, and then unwrapped by the MCF method. Finally, unwrapped differential interferograms were generated by adding the unwrapped residual phase to the range offset map. The unwrapped interferogram created by the offset-based method were compared with the unwrapped interferograms generated by the traditional MCF unwrapping method.

The difference between the offset-based and traditional methods were almost zero in most areas, except the areas near the fault line. The maximum difference in the ascending case was as large as 100.5 rad. at the fault line, which corresponds to a deformation of about 188.8 cm in the LOS direction. The maximum difference in the descending case was about 138.6 rad., which corresponds to a LOS deformation of about 260.4 cm. In addition, phase discontinuity and high decorrelation due to steep and complex deformation occurred in the 'linear surface rupture' area, and hence, the traditional method did not work correctly, while the offset-based method correctly measured the phase discontinuity as accurately as it estimated the LOS deformation in the highly decorrelated area. The achieved accuracies from the InSAR measurements were about 1.96 cm and 1.90 cm in the ascending and descending acquisitions, respectively.

The results showed that the offset-based method enables the measurement of valid deformations even in high-gradient and highly decorrelated deformation areas. Precise measurements in such deformation areas could allow for a better understanding of geological mechanisms

VI. ACKNOWLEDGMENT

The ALOS PALSAR-2 data used in this study are owned by Japan Aerospace Exploration Agency (JAXA), and the ALOS PALSAR-2 data were provided through the JAXA's ALOS-2 research program (RA4, PI No. 1412). And the GPS data were provided by Geospatial Information Authority of Japan.

REFERENCES

[1] E. Calais *et al.*, "Transpressional rupture of an unmapped fault during the 2010 Haiti earthquake," *Nature Geosci.*, vol. 3, no. 11, pp. 794–799, Oct. 2010.

[2] G. P. Hayes *et al.*, "Complex rupture during the 12 January 2010 Haiti earthquake," *Nature Geosci.*, vol. 3, no. 11, pp. 800–805, Oct. 2010.

[3] T. Kobayashi, M. Tobita, T. Nishimura, A. Suzuki, Y. Noguchi, and M. Yamanaka, "Crustal deformation map for the 2011 off the Pacific coast of Tohoku Earthquake, detected by InSAR analysis combined with GEONET data," *Earth, Planets Space*, vol. 63, p. 20, Sep. 2011. Accessed: Aug. 22, 2017, doi: 10.5047/eps.2011.06.043.

[4] M.-J. Jo, H.-S. Jung, and S.-H. Yun, "Retrieving precise three-dimensional deformation on the 2014 M6.0 South Napa earthquake by joint inversion of multi-sensor SAR," *Sci. Rep.*, vol. 7, Jul. 2017, Art. no. 5485. Accessed: Aug. 22, 2017, doi: 10.1038/s41598-017-06018-0.

[5] L. Moya, F. Yamazaki, W. Liu, and T. Chiba, "Calculation of coseismic displacement from lidar data in the 2016 Kumamoto, Japan, earthquake," *Natural Hazards Earth Syst. Sci.*, vol. 17, no. 1, pp. 143–156, Feb. 2017.

[6] S. Fujiwara *et al.*, "Small-displacement linear surface ruptures of the 2016 Kumamoto earthquake sequence detected by ALOS-2 SAR interferometry," *Earth, Planets Space*, vol. 68, p. 160, Sep. 2016. Accessed: Aug. 22, 2017, doi: 10.1186/s40623-016-0534-x.

[7] W.-K. Baek, H.-S. Jung, and S.-H. Chae, "Precise three-dimensional mapping of the 2016 Kumamoto earthquake through the integration of SAR interferometry and offset tracking," in *Proc. IGARSS*, Fort Worth, TX, USA, Jul. 2017, pp. 3822–3823.

[8] (2016). *The 2016 Kumamoto Earthquake: Crustal Deformation Around the Faults*. Accessed: Oct. 12, 2016. [Online]. Available: http://www.gsi.go.jp/cais/topic160428-index-e.html

[9] (2016). *Information on the Kumamoto Earthquake in Heisei 28*. Aceesed: Oct. 12, 2016. [Online]. Available: http://www.gsi.go.jp/BOUSAI/H27-kumamoto-earthquake-index.html

[10] Y. Himematsu and M. Furuya, "Fault source model for the 2016 Kumamoto earthquake sequence based on ALOS-2/PALSAR-2 pixel-offset data: Evidence for dynamic slip partitioning," *Earth, Planets Space*, vol. 68, p. 169, Oct. 2016. Accessed: Aug. 22, 2017, doi: 10.1186/s40623-016-0545-7.

[11] S.-H. Yun, H. Zebker, P. Segall, A. Hooper, and M. Poland, "Interferogram formation in the presence of complex and large deformation," *Geophys. Res. Lett.*, vol. 34, p. L12305, Jun. 2007. Accessed: Aug. 12, 2017, doi: 10.1029/2007GL029745.

[12] H. S. Jung, Z. Lu, J. S. Won, M. P. Poland, and A. Miklius, "Mapping three-dimensional surface deformation by combining multiple-aperture interferometry and conventional interferometry: Application to the June 2007 eruption of Kilauea Volcano, Hawaii," *IEEE Geosci. Remote Sens. Lett.*, vol. 8, no. 1, pp. 34–38, Jul. 2011.

[13] M.-J. Jo, H.-S. Jung, J.-S. Won, and P. Lundgren, "Measurement of three-dimensional surface deformation by Cosmo-SkyMed X-band radar interferometry: Application to the March 2011 Kamoamoa fissure eruption, Kilauea Volcano, Hawai'i," *Remote Sens. Environ.*, vol. 169, pp. 176–191, Nov. 2015.

[14] M.-J. Jo, H.-S. Jung, and J.-S. Won, "Measurement of precise three-dimensional volcanic deformations via TerraSAR-X synthetic aperture radar interferometry," *Remote Sens. Environ.*, vol. 192, pp. 228–237, Apr. 2017.

[15] Z. Lu, D. Mann, J. T. Freymueller, and D. J. Meyer, "Synthetic aperture radar interferometry of Okmok Volcano, Alaska: Radar observations," *J. Geophys. Res. B, Solid Earth*, vol. 105, no. B5, pp. 10791–10806, May 2000.

[16] R. DesRoches, M. Comerio, M. Eberhard, W. Mooney, and G. J. Rix, "Overview of the 2010 Haiti earthquake," *Earthq. Spectra*, vol. 27, no. S1, pp. S1–S21, Oct. 2011.

[17] H.-S. Jung, J.-S. Won, and S.-W. Kim, "An improvement of the performance of multiple-aperture SAR interferometry (MAI)," *IEEE Trans. Geosci. Remote Sens.*, vol. 47, no. 8, pp. 2859–2869, Apr. 2009.

[18] H.-S. Jung, S.-H. Yun, and M.-J. Jo, "An improvement of multiple-aperture sar interferometry performance in the presence of complex and large line-of-sight deformation," *IEEE J. Sel. Topics Appl. Earth Observ. Remote Sens.*, vol. 8, no. 4, pp. 1743–1752, Feb. 2015.

[19] H. Huang and Q. Wang, "A method of filtering and unwrapping SAR interferometric phase based on nonlinear phase model," *Prog. Electromagn. Res.*, vol. 144, no. 1, pp. 67–78, 2014.

[20] P. LÃşpez-Quiroz, M.-P. Doin, F. Tupin, P. Briole, and J.-M. Nicolas, "Time series analysis of Mexico City subsidence constrained by radar interferometry," *J. Appl. Geophys.*, vol. 69, no. 1, pp. 1–15, Sep. 2009.

[21] J. J. Martinez-Espla, T. Martinez-Marin, and J. M. Lopez-Sanchez, "Using a grid-based filter to solve InSAR phase unwrapping," *IEEE Trans. Geosci. Remote Sens.*, vol. 5, no. 2, pp. 147–151, Apr. 2008.

[22] H. Rott, M. Stuefer, A. Siegel, P. Skvarca, and A. Eckstaller, "Mass fluxes and dynamics of Moreno Glacier, Southern Patagonia Icefield," *Geophys. Res. Lett.*, vol. 25, no. 9, pp. 1407–1410, May 1998.

[23] T. Strozzi, A. Luckman, T. Murray, U. Wegmuller, and C. L. Werner, "Glacier motion estimation using SAR offset-tracking procedures," *IEEE Trans. Geosci. Remote Sens.*, vol. 40, no. 11, pp. 2384–2391, Nov. 2002.

[24] J. Li, Z. W. Li, X. L. Ding, Q. J. Wang, J. J. Zhu, and C. C. Wang, "Investigating mountain glacier motion with the method of SAR intensity-tracking: Removal of topographic effects and analysis of the dynamic patterns," *Earth Sci. Rev.*, vol. 138, pp. 179–195, Nov. 2014.

[25] S.-H. Chae, W.-J. Lee, H.-S. Jung, and L. Zhang, "Ionospheric correction of L-band SAR offset measurements for the precise observation of glacier velocity variations on Novaya Zemlya," *IEEE J. Sel. Topics Appl. Earth Observ. Remote Sens.*, vol. 10, no. 8, pp. 3591–3603, Apr. 2017.

[26] H.-S. Jung, W.-J. Lee, and L. Zhang, "Theoretical accuracy of along-track displacement measurements from multiple-aperture interferometry (MAI)," *Sensors*, vol. 14, no. 9, pp. 17703–17724, Sep. 2014.

[27] H. A. Zebker and J. Villasenor, "Decorrelation in interferometric radar echoes," *IEEE Trans. Geosci. Remote Sens.*, vol. 30, no. 5, pp. 950–959, Sep. 1992.

[28] M. Costantini, P. A. Rosen, and C. L. Werner, "Preventing and masking out unreliable results for critical quantitative applications of phase unwrapping," in *Proc. IGARSS*, Honolulu, HI, USA, Jul. 2000, pp. 3199–3201.

[29] R. M. Goldstein, H. A. Zebker, and C. L. Werner, "Satellite radar interferometry: Two-dimensional phase unwrapping," *Radio Sci.*, vol. 23, no. 4, pp. 713–720, Jul./Aug. 1988.

[30] R. M. Goldstein and C. L. Werner, "Radar interferogram filtering for geophysical applications," *Geophys. Res. Lett.*, vol. 25, no. 21, pp. 4035–4038, Nov. 1998.

[31] M. Costantini, "A novel phase unwrapping method based on network programming," *IEEE Trans. Geosci. Remote Sens.*, vol. 36, no. 3, pp. 813–821, May 1998.

[32] M. Costantini and P. A. Rosen, "A generalized phase unwrapping approach for sparse data," in *Proc. IGARSS*, Hamberg, Germany, Jun./Jul. 1999, pp. 267–269.

[33] L. Ge, H. Wang, H. C. Chang, and C. Rizos, "Linear combinations for differential radar interferometry," in *Observing Our Changing Earth* (International Association of Geodesy Symposia), vol. 133. Berlin, Germany: Springer, 2009, pp. 825–829.

[34] W.-J. Lee, H.-S. Jung, and Z. Lu, "Application of ERS and Envisat cross-interferometry to generation and accuracy assessment of digital elevation model over northern Alaska," *J. Appl. Remote Sens.*, vol. 9, no. 1, pp. 096065-1–096065-15, Apr. 2015.

[35] A. Buades, B. Coll, and J. M. Morel, "A non-local algorithm for image denoising," in *Proc. IEEE Comput. Soc. Conf. Comput. Vis. Pattern Recognit.*, San Diego, CA, USA, Jun. 2005, pp. 60–65.

[36] D. Kim and H.-S. Jung, "Oil spill detection from RADARSAT-2 SAR image using non-local means filter," *Korean Remote Sens. Soc.*, vol. 33, pp. 61–67, Feb. 2017.

[37] H.-S. Jung, D.-T. Lee, Z. Lu, and J.-S. Won, "Ionospheric correction of SAR interferograms by multiple-aperture interferometry," *IEEE Trans. Geosci. Remote Sens.*, vol. 51, no. 5, pp. 3191–3199, May 2013.
[38] Z. Liu, H.-S. Jung, and Z. Lu, "Joint correction of ionosphere noise and orbital error in L-band SAR interferometry of interseismic deformation in southern California," *IEEE Trans. Geosci. Remote Sens.*, vol. 52, no. 6, pp. 3421–3427, Jun. 2014.
[39] H.-S. Jung and W.-J. Lee, "An improvement of ionospheric phase correction by multiple-aperture interferometry," *IEEE Trans. Geosci. Remote Sens.*, vol. 53, no. 9, pp. 4952–4960, Sep. 2015.

WON-KYUNG BAEK was born in Daegu, South Korea, in 1991. He received the B.S and M.S degrees in geoinformatics and remote sensing from the University of Seoul, South Korea, in 2015 and 2017, respectively, where he is currently pursuing the Ph.D. degree in geoinformatics and remote sensing.

His research interests include multi-temporal and 3-D ground deformation measurements using phase- and pixel-based SAR measurement approaches, error mitigation in the SAR-based ground deformation measurements, and recently efficient procedure to unwrap large and complex SAR interferograms using offset tracking.

HYUNG-SUP JUNG (M'09–SM'16) received the M.S. degree in geophysics and the Ph.D. degree in remote sensing from Yonsei University, Seoul, South Korea, in 1998 and 2007, respectively.

He is currently an Associate Professor with the Department of Geoinfomatics, University of Seoul. His primary research interests cover the development of algorithms related to synthetic aperture radar (SAR), SAR interferometry (InSAR), multiple-aperture InSAR (MAI), and multitemporal InSAR, automated geometric correction of multisensor images, and multisensor image processing and fusion, thermal remote sensing, and multitemporal optical and thermal sensing. He has been developing algorithms for remote sensing applications related to 3-D deformation mapping by combining MAI and InSAR, 2-D surface velocity estimation by combining MAI and along-track interferometry, MAI-based ionospheric correction of radar interferograms, multisensor fusion by the integration of optic and SAR, SAR and thermal, and optic and thermal images, automated geometric correction for optic and SAR images, and Earth's surface variation monitoring, such as urban subsidence monitoring, glacier monitoring, volcano monitoring, deforestation monitoring, forest mapping, forest fire mapping, and snow depth estimation.

SUNG-HO CHAE received the M.S. degree in geoinformatics from the University of Seoul, South Korea, in 2016, where he is currently pursuing the Ph.D. degree with the Department of Geoinformatics.

His research interests include improving the measurement performance of the conventional SAR offset tracking method and advanced 3-D surface deformation mapping by the integration of interferometric SAR (InSAR) and multiple-aperture InSAR (MAI) measurements. He currently focuses on retrieving 3-D glacier motions using InSAR, MAI, and SAR offset tracking methods.